Journal for ImmunoTherapy of Cancer

Structural insights into engineering a T-cell receptor targeting MAGE-A10 with higher affinity and specificity for cancer immunotherapy

Philip C Simister, Ellen C Border, João F Vieira, Nicholas J Pumphrey

To cite: Simister PC, Border EC, Vieira JF, *et al*. Structural insights into engineering a T-cell receptor targeting MAGE-A10 with higher affinity and specificity for cancer immunotherapy. *Journal for ImmunoTherapy of Cancer* 2022;**10**:e004600. doi:10.1136/jitc-2022-004600

Accepted 17 May 2022

Adaptimmune, Abingdon, Oxfordshire, UK

Correspondence to
Dr Philip C Simister;
Philip.Simister@adaptimmune.com

ABSTRACT

Background T-cell receptor (TCR) immunotherapy is becoming a viable modality in cancer treatment with efficacy in clinical trials. The safety of patients is paramount, so innovative cell engineering methods are being employed to exploit adaptive immunity while controlling the factors governing antigen receptor (ie, TCR) specificity and cross-reactivity. We recently reported a TCR engineering campaign and selectivity profiling assay (X-scan) targeting a melanoma antigen gene (MAGE)-A10 peptide. This helped to distinguish between two well-performing TCRs based on cross-reactivity potential during preclinical drug evaluation, allowing one to be advanced to T-cell immunotherapeutic clinical trials. Here, we present three-dimensional structural information on those TCRs, highlighting engineering improvements and molecular mechanisms likely underpinning differential selectivity.

Methods Parental and engineered TCRs were purified and crystallized either alone or complexed to human leucocyte antigen (HLA)-A*02:01 presenting the MAGE-A10 9-mer peptide, GLYDGMEHL (pHLA/MAGE-A10-9). Using X-ray diffraction, we solved four high-resolution crystal structures and evaluated them relative to previously reported functional results.

Results The unligated parental TCR displayed similar complementarity-determining region (CDR) loop conformations when bound to pHLA/MAGE-A10-9; a rigid-body movement of TCR beta chain variable domain (TRBV) relative to TCR alpha chain variable domain helped optimal pHLA engagement. This first view of an HLA-bound MAGE-A10 peptide revealed an intrachain non-covalent 'staple' between peptide Tyr3 and Glu7. A subtle Glu31-Asp mutation in βCDR1 of the parental TCR generated a high-affinity derivative. Its pHLA-complexed structure shows that the shorter Asp leans toward the pHLA with resulting rigid-body TRBV shift, creating localized changes around the peptide's C-terminus. Structural comparison with a less selective TCR indicated that differential cross-reactivity to MAGE-A10 peptide variants is most readily explained by alterations in surface electrostatics, and the size and geometry of TCR-peptide interfacial cavities.

Conclusions Modest changes in engineered TCRs targeting MAGE-A10 produced significantly different properties. Conformational invariance of TCR and antigen peptide plus more space-filling CDR loop sequences may be desirable properties for clinically relevant TCR–pHLA systems to reduce the likelihood of structurally similar peptide mimics being tolerated by a TCR. Such properties may partially explain why the affinity-enhanced, in vitro-selected TCR has been generally well tolerated in patients.

WHAT IS ALREADY KNOWN ON THIS TOPIC

⇒ T-cell receptor (TCR) T-cell immunotherapy is becoming a viable modality in cancer treatment with efficacy in clinical trials. Structural information on TCR-target complexes can reveal molecular insights underpinning differential selectivity and affinity, but there is a paucity of information on clinically relevant TCRs and their target specificity.

WHAT THIS STUDY ADDS

⇒ New crystal structures help to explain how affinity enhancement and specificity profiling have been of benefit in developing an engineered TCR targeting a MAGE-A10 peptide presented by HLA-A*02:01 that displayed an acceptable safety profile in clinical trials.

HOW THIS STUDY MIGHT AFFECT RESEARCH, PRACTICE OR POLICY

⇒ This study provides further rationale that, with careful selection of engineered TCR candidates and selectivity screening, the likelihood of cross-reactivity can be minimized to generate clinically safe affinity-enhanced TCR T-cell therapies.

BACKGROUND

Cancer testis antigens are long established as advantageous targets for adoptive cell therapy, due to their restricted expression profiles in normal, healthy human tissue contrasted with high overexpressed levels in specific cancers with evident immunogenicity.[1] We and others have exploited this class of protein target to generate experimental cell-based immunotherapies that are currently under evaluation in a clinical setting, with cancer testis antigens (the most common target class in solid tumors) accounting for ~50% of all targets.[2]

Various members of the melanoma antigen gene (MAGE) family are among these

productive targets; specifically, the type 1 subset (subfamilies A, B, and C) is undergoing clinical evaluation, with two studies having MAGE-A10 as the sole anticancer target.[3] MAGE proteins are increasingly being understood as not merely byproducts of tumor growth, but also as key drivers in oncogenesis.[4] However, due care must be taken to assess the potential for cross-reactive homologies between the closely related type 1 family members. For instance, an MAGE-A3/MAGE-A12 peptide target similarity resulted in fatal brain toxicity.[5] Additionally, general off-target cross-reactivity is a major concern for any T-cell immunotherapeutic target as occurred when a T-cell receptor (TCR) against another MAGE-A3 peptide cross-reacted to a structurally similar Titin peptide in heart muscle cardiomyocytes, resulting in fatal cardiac toxicity.[6]

From such studies, it has been surmised that a higher risk of cross-reactivity is associated with affinity enhancement of TCRs,[7] be they endogenous and thymically selected in origin, or (perhaps to a greater extent) non-thymically selected TCRs as might be generated in the laboratory (eg, from display library technologies such as phage,[8] yeast,[9] or mammalian cell systems). However, counterexamples of safer engineered T-cell products are emerging from advancing clinical trials, in particular against cancer testis antigen targets such as New York esophageal squamous cell carcinoma 1 (NY-ESO-1), MAGE-A4, and MAGE-A10.[10–12] Increasingly, more refined preclinical safety methods are being employed to screen the cross-reactome in order to minimize the likelihood of taking to the clinic a TCR T-cell product with associated off-target reactivities.[13–17] This is in addition to the generic problem in target validation of avoiding on-target, off-tumor reactivity and toxicity, whereby a safe therapeutic window of target expression ensures selective targeting of tumor over normal cells.

The appeal of phage and other display technologies for TCR discovery over alternative methods (eg, isolation of natural blood products, such as patient tumor-infiltrating lymphocytes and donor peripheral blood mononuclear cells) lies in their ease and speed of implementation, low cost, and effectiveness. The ability to use their outputs and engineer in enhanced TCR functionality (tumor cell lytic activity) allows relatively rapid access to more potent TCRs that surpass the restrictions and limitations of the thymus. This process does, however, require careful monitoring of developed TCR products, as mentioned, for specificity and safety.

In our recent report,[13] we outlined a process from TCR discovery by phage display to selection of two leading engineered (affinity-enhanced) TCRs (named c756 and c796) from different parental TCRs with functional activity against MAGE-A10 GLYDGMEHL$^{254\text{-}262}$ antigenic peptide. These TCRs were otherwise quite similar in affinity as measured in vitro by surface plasmon resonance, and in cellular potency by interferon-γ release enzyme-linked immunospot assay, with c796 a little more potent (for c796 and c756, respectively: dissociation constant 370 nM vs 610 nM; effective concentration 50% 0.32 nM vs 0.50 nM).[13]

Importantly, to evaluate their propensity to tolerate non-canonical peptide sequence variants, and thus to distinguish better between these two TCRs based on target selectivity, we reported an X-scan screen. At each residue position of the nonameric human leucocyte antigen (HLA)-bound peptide, the wild-type residue was systematically substituted for 19 other amino acids, and the functional responses measured to these peptide variants using T-cells transduced with c756 or c796 TCRs. This type of specificity profiling is useful for characterizing the binding promiscuity of a TCR and can provide valuable information on binding hotspots on a peptide.

Higher selectivity was demonstrated with the c796 TCR due to its reduced tolerance to mutant peptides varying in the central, more surface-exposed peptide region compared with c756 TCR. The c796 TCR ultimately formed the basis of Adaptimmune's ADP-A2M10 specific peptide enhanced affinity receptor (SPEAR) T-cell therapy that entered phase I/II clinical trials in a triple tumor study (melanoma, urothelial, or head and neck cancers),[18] and a non-small cell lung cancer study.[19] This TCR T-cell therapy has proven to be generally well tolerated in those clinical tests, with a manageable toxicity profile.[12]

We reveal that the c796 TCR was engineered by incorporating a single conservative mutation into the parental TCR, c728, which resulted in a ~sixfold increase in binding affinity to peptide–HLA complex (pHLA) compared with the parental as measured by surface plasmon resonance.[13] Thus, we wished to understand at the molecular level how this subtle change could affect pHLA binding. Moreover, we questioned what protein structural differences at the peptide-binding interfaces of the engineered c796 TCR, compared with c756 TCR, might account for different X-scan cross-reactivity/selectivity profiles. Here, we present detailed three-dimensional (3D) information on our reported engineering campaign[13] from the structural perspective of four high-resolution crystal structures: the parental TCR, c728; its derivative engineered TCR, c796; and the potentially more cross-reactive engineered TCR, c756 (from a different parent), each in complex with pHLA (HLA-A*02:01/MAGE-A10-9). We also include a comparison with the c728 parental TCR structure alone as an example of the unligated TCR state. The new structural data enhance our understanding of TCR engagement and suggest TCR and pHLA characteristics that may be beneficial in terms of safety across TCR T-cell therapies more generally.

METHODS

Molecular biology

Bacterial expression plasmids harboring the genes for β-2-microglobulin (residues 1–99) as well as HLA-A*02:01 alpha chain (residues 1-276), TCR alpha chains, and TCR beta chains lacking transmembrane regions or signal

peptides were generated similarly to those previously described,[13] except with no additional purification tags present.

Protein production

TCR chains were expressed individually in *E. coli* Rosetta cells (Novagen/Merck, Germany) as insoluble inclusion bodies and purified largely as described.[13] Briefly, TCRs were produced by refolding in 8M urea and slow dialysis. A molar ratio of 1.2:1 alpha to beta chain was mixed under denaturing conditions and dialyzed for up to 48 hours in 10 mM Tris pH 8.0 before performing ion exchange chromatography (HiTrap MonoQ; Cytiva, USA), followed by size-exclusion chromatography (HR 16/600 or HR 10/300 columns; GE Healthcare, UK). pHLA was produced similarly but with a 1:2 molar ratio of HLA alpha chain to β-2-microglobulin and an excess added of the MAGE-A10-GLY 9-mer peptide (>98% purity; Peptide Protein Research, UK) with up to 60 hours of refolding with dialysis, followed by ion exchange chromatography and size-exclusion chromatography. TCR–pHLA complexes were formed by mixing equimolar quantities of pHLA and TCR, and final purification by size-exclusion chromatography in phosphate-buffered saline.

Protein crystallization and X-ray diffraction

Proteins (TCR or TCR–pHLA complexes) were centrifuged before setting up crystallization trials. The final concentrations ranged between 10 and 20 mg/mL. All proteins were mixed in 96-well Greiner plates either as 2:1, 1:1, or 1:2 ratios, with the screen solution (mother liquor) from commercial primary sparse-matrix screens using a Mosquito liquid handler (SPT Labtech, UK). Final drop volumes were 200 nL; plates were incubated at 20°C in a Rock Imager (Formulatrix, USA). c728 TCR at 19 mg/mL crystallized when mixed 1:2 with 0.2 M lithium sulfate, 0.1 M MES pH 6.0, 20 % w/v PEG 4000 (ProPlex screen, Molecular Dimensions, UK). The following relate to trials using the PACT Premier screen (Molecular Dimensions, UK): c728 TCR–pHLA (at 10.7 mg/mL) crystals grew from 0.02 M sodium/potassium phosphate, 0.1 M bis-Tris propane pH 6.5, 20% w/v PEG 3350; c756 TCR–pHLA (at 10.3 mg/mL) crystals grew from 0.2 M sodium chloride, 0.1 M MES pH 6.0, 20% w/v PEG 6000; c796 TCR–pHLA (at 10.2 mg/mL) crystals grew in 0.2 M ammonium chloride, 0.1 M HEPES pH 7.0, 20% w/v PEG 6000. All crystals were harvested by exchanging first into mother liquor supplemented with 20% glycerol before cryopreservation in liquid nitrogen.

Synchrotron X-ray data were collected with an X-ray wavelength of 0.9763 Å at beamline I03 by Diamond Light Source Industrial Liaison Unit and beamline staff.

Data processing and model refinement

X-ray data were processed within the *CCP4i* suite[20] by first integrating diffraction image spots with *iMOSFLM*[21] or *DIALS*[22] in the *XIA2* pipeline,[23] data reduced with *AIMLESS*[24] and then phasing by molecular replacement using *PHASER*.[25] The TCR structure with Protein Data Bank (PDB) code 3QEU[26] was used as a search model for phasing the TCR component of the c796 TCR–pHLA/MAGE-A10-9 complex, but with the complementarity-determining region (CDR) 3 loops removed from the model. The pHLA component was identified using a high-resolution HLA-A*02:01 structure presenting MAGE-A4 peptide (PDB code: 1I4F[27]) as the molecular replacement search model, but with the peptide removed.

Models were refined iteratively with several rounds of automated refinement in *REFMAC5*[28] and manual model building in *Coot*.[29] The refined c796 TCR–pHLA complex model was subsequently used to solve the other structures. The structure of the c728 TCR alone and in complex, and that of c796 TCR in complex with pHLA/MAGE-A10-9, had peptide Phi/Psi angles for 100% of residues in the allowed or favorable regions of the Ramachandran plot according to *Molprobity* analysis.[30] The highest resolution c756 TCR–pHLA complex structure had all but one residue within the most favorable or allowed regions (table 1). The higher-energy residue was Ala97 in the βCDR3 loop and was precisely defined by the electron density in the middle of the TCR–pHLA-binding interface. To note, the equivalent residue is a Thr in the c728/c796 structural complexes and was borderline in the 'allowed' region.

RESULTS

Comparison of HLA-A*02:01 presentation of MAGE-A10 and MAGE-A4 peptides

To understand better the mechanism of action of our parental and engineered TCRs, we aimed to obtain 3D structural data. We set up crystallization trials with c728, c756, and c796 TCRs in complex with HLA-A*02:01 presenting the cancer target MAGE-A10 9-mer peptide (full sequence: GLYDGMEHL), here termed pHLA/MAGE-A10-9. We also crystallized the parental TCR (c728) alone. This produced thin crystalline plates diffracting to 2.3 Å resolution. We then obtained larger single crystals of c728 TCR in complex with pHLA/MAGE-A10-9, solved to high resolution for a TCR–pHLA complex (1.8 Å). This represents the first reported view of a MAGE-A10 peptide bound to an HLA molecule. We did not obtain diffraction-quality crystals of the pHLA alone in the time available.

There is similarity in the local structural arrangement adopted by the MAGE-A10 9-mer peptide and the MAGE-A4 10-mer counterpart (GVYDGREHTV) when crystallized (PDB codes: 1I4F & 6TRO), but due to the shorter length of MAGE-A10-9, there is no pronounced central bulge as for the equivalent MAGE-A4 peptide (figure 1). A common feature of these MAGE peptides is the bulky Tyr in the p3 position (p-Tyr3). This residue embeds itself below the surface of the peptide toward the base and side of the HLA peptide groove. It electrostatically bonds across to the negatively charged p-Glu7

Table 1 X-ray data processing and model refinement information

Parameter	Protein crystallographic details			
Data processing				
Protein content	c728 TCR	c728 TCR and HLA-A*02:01/ MAGEA10-GVY-9	c796 TCR and HLA-A*02:01/ MAGEA10-GVY-9	c756 TCR and HLA-A*02:01/ MAGEA10-GVY-9
Space group	P1	P1	$P2_1$	$P2_1$
Unit cell parameters:				
Lengths a, b, c (Å)	54.9, 59.2, 86.0	54.1, 95.8, 106.3	54.3, 77.5, 115.1	54.2, 77.4, 116.7
Angles α, β, λ (°)	101.9, 105.9, 104.7	109.2, 96.5, 99.7	90.00, 102.9, 90.0	90.0, 102.7, 90.0
Resolution range (Å)	79.0–2.27	81.9–1.82	77.5–2.04	77.5–1.54
No. of unique reflections	38348	158062	59081	134415
I/σ(I)	4.3 (2.3)	4.7 (0.7)	5.7 (1.6)	6.4 (1.0)
R_{meas}	16.6 (29.7)	13.9 (95.0)	14.5 (90.4)	10.5 (138.1)
Multiplicity	1.5 (1.5)	1.5 (1.4)	2.9 (2.8)	3.2 (3.1)
$CC_{1/2}$	0.957 (0.898)	0.986 (0.464)	0.988 (0.728)	0.995 (0.331)
Completeness (%)	86.2 (84.5)	90.2 (87.5)	99.3 (98.7)	96.9 (95.8)
Model details and refinement statistics				
R_{work} (%)	19.2 (25.5)	20.2 (33.6)	18.6 (29.3)	20.2 (33.9)
R_{free} (%)	25.2 (31.9)	22.9 (33.4)	23.6 (30.9)	23.6 (32.1)
No. of atoms	7061	13735	6829	7098
No. of waters	299	637	349	528
No. of copies in asymmetric unit	2	2	1	1
Ramachandran plot (%)				
Favored regions	96.9	97.4	96.3	97.5
Allowed regions	3.1	2.6	3.7	2.4
Outliers	0	0	0	0.1

HLA, human leucocyte antigen; TCR, T-cell receptor.

residue on its own peptide chain. The MAGE-A10 peptide is clearly visible (figures 2 and 3) looking down on the TCR as the peptide sits between TCR alpha chain variable domain (TRAV) and TCR beta chain variable domain (TRBV), with the HLA removed from view in figure 3, and the HLA-binding part of the peptide exposed at the surface. Although we were unable to obtain sufficiently high-resolution crystals of pHLA/MAGE-A10-9 alone, the peptide—with self-interactions and embedded docking position—appears to be particularly stable. The intra-chain hydrogen bonding results in a unique local structure, involving the bulky hydrophobic tyrosyl group and aliphatic portion of p-Glu7 in close contact with the HLA-binding groove.

Parental TCR retains its overall CDR loop geometries upon binding to pHLA

The unbound or 'free' parental TCR (c728) crystallized with two molecules in the crystallographic asymmetric unit. After protein model building, one of the two TCR copies had better-defined CDR3 loop density, and thus we used this copy to compare the TCR with its pHLA-bound state. In the complex, as would be expected on docking into a more restricted conformation, all TCR CDR loop residues were visible with clear electron density. Of note, the c728 TCR–pHLA complex also crystallized with two molecules in the asymmetric unit, although there were no remarkable differences between the two at the pHLA-binding interface. On superposition, it was clear that the TCR conformation in the pHLA-bound form was nearly identical to its unbound state.

The TRAV domain backbone in particular was largely conformationally invariant between states, with minimal deviation of all CDR loop positions and also the entire variable domain. The TRBV domain also maintained the same general trajectories of its CDR loops, but a rigid-body-like concerted movement of all βCDR loops relative to the TRAV domain occurred. The TRBV has pivoted a little around a central axis between TCR chains, displaying a maximal shift of 2.7Å at the outer edge (figure 2). This has allowed more favorable positioning with respect to the pHLA α1 and α2 helices and peptide; local side-chain movements of various residues in the vicinity of these segments are discernible.

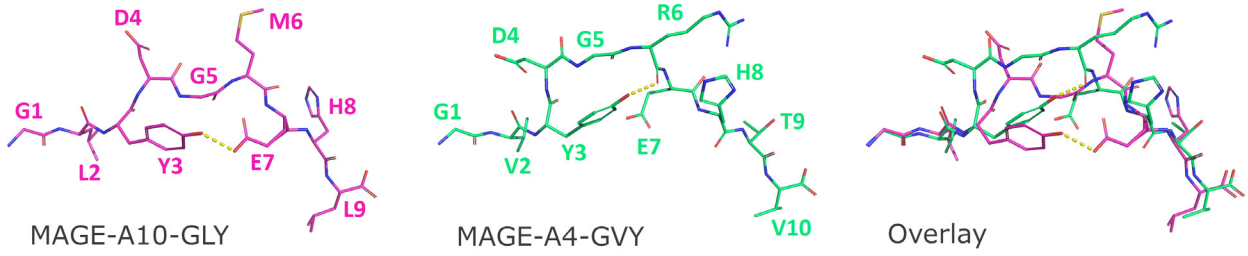

Figure 1 Structures of melanoma-associated antigen (MAGE)-A10 GLYDGMEHL peptide and the published MAGE-A4 GVYDGREHTV homolog. The MAGE peptides as crystallized within the T-cell receptor (TCR)–peptide–human leucocyte antigen (pHLA) complexes are depicted in isolation, with MAGE-A10 9-mer from this study compared with the MAGE-A4 10-mer peptide from a recently reported structure (Protein Data Bank code: 6TRO).[42] In this orientation, though removed from view, the TCR would be on top and HLA below. MAGE-A10 presents two key side-chains to the TCR: p-Asp4 and p-Met6, like a 2-pin plug. Curiously, the bulky p-Tyr3 (Y3) prefers to bend into the HLA's peptide-binding groove in both MAGE peptides and H-bond to a position further along the peptide chain: in MAGE-A10 to the side-chain of p-Glu7, which also avoids TCR exposure; in MAGE-A4 to the backbone nitrogen of p-Arg6. This internal non-covalent stapling and side-chain positioning with increased HLA contact might be expected to bring added conformational stability within the peptides themselves and to the pHLA complex. Although highly similar at the 1D sequence level, the two peptides are otherwise structurally dissimilar in the context of an HLA, due to the MAGE-A4 10-mer adopting a central bulge to accommodate the extra amino acid, which influenced the docking location over the peptide's N-terminus of the reported GVY01 TCR.[42] Image generated with PyMOL (Schrödinger, New York, New York, USA).

Mode of TCR engagement to the MAGE-A10 peptide

The parental TCR engaged onto the MAGE-A10[1] GLYDGMEHL[9] peptide using two main features: p-Asp4 and p-Met6 (figure 2B). These central side-chains protrude out toward the TCR. p-Met6 pokes into a cavity between the TCR chains, flanked on four sides by hydrophobic interactions from two αCDR3 Arg residues (amino acids 93 and 98), which can also H-bond to the peptide backbone; βCDR1 Tyr32; and the central part of the βCDR3 backbone near to Thr97 (figure 2C).

αCDR3 Arg98 is heavily implicated in peptide engagement, as it also uses its positive charge to couple electrostatically to p-Asp4, which provides an additional anchor point for the p-Gly5 backbone nitrogen. This mode of docking—like a two-pin MAGE-A10 peptide plug into a TCR socket—was seen consistently for all TCRs mentioned in this report (see below).

An engineered conservative mutation greatly impacted TCR affinity and potency

As previously reported,[13] the parental c728 TCR was engineered to a high-affinity form (c796), which passed our preclinical safety program and entered phase I/II clinical trials[18 19]; it is currently undergoing post-study evaluation. For successful engineering, it sufficed to switch residue 31 in βCDR1 from Glu (E) to Asp (D), retaining the negative charge to gain a ~sixfold increase in affinity, which also maintained high specificity to the pHLA/MAGE-A10-9 target. Crystallography allowed investigation of why such a minimal change—that is, the removal of a single backbone -CH_2 unit and consequential shortening of a βCDR1 residue side-chain—might cause this affinity increase.

Large, single crystals of the higher-affinity engineered c796 TCR in complex with pHLA/MAGE-A10-9 grew readily as thick plates up to 0.5 mm in length and diffracted to 2.1 Å resolution. Superimposition of the two complexes through structural alignment of the peptide-binding domain of the HLA alpha chain (residues 1–180 only) allowed clearer visualization of changes at the binding interface. In this overlay, the peptides structurally aligned with barely noticeable differences in their positions (note, HLA chains are removed from view in figure 3A). The following observations are evident:

1. The c796 TRAV domain CDR loops adopt the same positions as seen in the c728 TCR complex, which is unsurprising, given that no modification was engineered into the αCDR1-3 loops. However, the shortening of the βCDR1 Glu side-chain to Asp allows a direction change for the side-chain to fit into the space adjacent to the peptide's C-terminal end. Glu in the parental TCR is slightly too long, whereas Asp in the engineered c796 derivative TCR permits this shifted peptide-leaning conformation (figure 3A).
2. In swinging toward the pHLA, the modified Asp brings with it the entire βCDR1 loop, with a maximal shift of ~1.2 Å, and each βCDR loop also moves in concert with βCDR1 (ie, as an apparent rigid body indicating loop interconnectivity). Thus, the upper part of the TRBV region is pulled in through inter-βCDR loop bonding networks by the engineered Asp.
3. The gap created by the inability of the c728 TCR Glu residue to bend toward the pHLA without a clash is obligatorily filled with solvent (several water molecules occupy the void, figure 3B, left and middle panels). The side-chain of the Asp mutant now lying in this space has necessarily caused restructuring of the interfacial solvent network at this site, with water removal allowing closer contact with pHLA at the mutated position. In the new arrangement, because the TRBV can move in marginally closer toward the pHLA, new contacts to the TCR become possible. While still not

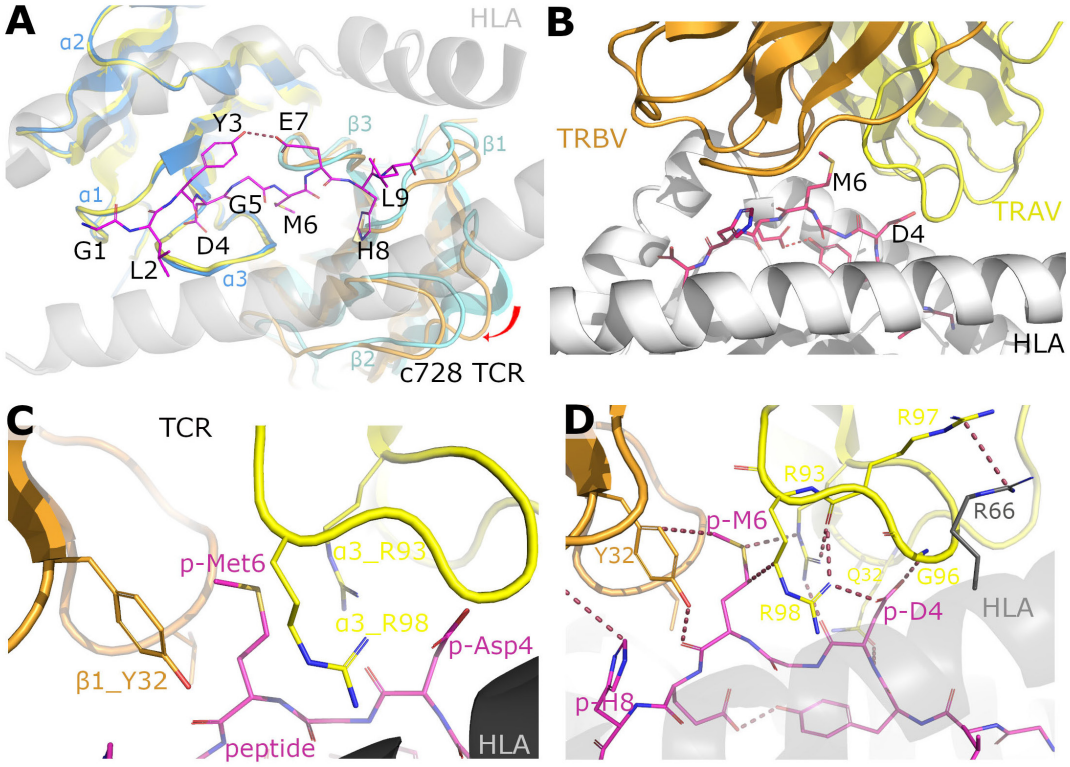

Figure 2 Views of parental c728 T-cell receptors (TCRs) before and after peptide–human leucocyte antigen (pHLA)/melanoma-associated antigen (MAGE)-A10-9 engagement. TCRs were superimposed on their TCR alpha chain variable domains (TRAV) (c728, pale yellow—unbound; c796, yellow—bound), which permits the interchain movement to be visualized with respect to the TCR beta chain variable domain (TRBV; note, the TRAVs had a lower self root-mean-squared deviation than TBRV, indicating higher internal rigidity/conformational invariance). The TRAVs had barely any shift, even α complementarity-determining region (CDR)3. With the TRAV fixed, there is a relative shift of the parental c728 TCR TRBV domain (unbound, cyan) on pHLA engagement to its new position (bound, orange; red arrow). This movement is not large, less than 3 Å at its widest point distant from an apparent hinging axis down through the central TRAV–TRBV interface. In (A), the pHLA is on top and the TCR below; the α1 and α2 helices (white) are made partially transparent to see the TCR beneath. The rotation of TRBV is necessary to avoid clashes with the HLA helices in order to dock. The MAGE-A10 peptide (GLYDGMEHL; pink sticks) buries its bulky Tyr3 side-chain into the HLA peptide-binding groove away from TCR but reaches under/across with an H-bond (red dashed line) to the buried p-Glu7 achieving a non-covalent cyclization arrangement resembling a self-staple. The TCR docks in a very central position with little tilt. (B) View of the interface from the side with c728 TCR on top bound to pHLA underneath, illustrating the 2-pin plug engagement. p-Met6 protrudes directly up between the TCR chains, and p-Asp4 points off to the side into a shallower pocket in the TRAV domain (see also figure 4B). (C and D) Detail at the c728 TCR–MAGE-A10 peptide interface. p-Met6 slots into a tunnel flanked by two of three αCDR3 Arg residues (R93 and R98), βCDR1_Y32, and the backbone of βCDR3_T97. The αCDR3 Arg residues engage at multiple contact points, including p-Asp4 side-chain and backbone. Additional TCR–peptide or TCR–HLA contacts are annotated in (D). Images generated with PyMOL (Schrödinger, New York, New York, USA).

directly bound to pHLA, the Asp residue can H-bond to an invariant water as seen in all three complexes discussed in this report. Differential H-bonding opportunities are depicted for c728 and c796 (figure 3B, left and middle panels). The effect of moving TRBV closer to the pHLA and other differential contacts are more easily appreciated in the zoomed view of each complexed TCR when overlaid. For example, TRAV Lys72 in the interloop framework region, which resides too far from the pHLA in the parental TCR, becomes shifted by 0.9 Å to enable H-bonding to a well-defined solvent molecule that can act as a TCR–pHLA bridge (figure 3B, right panel). Although we have not attempted to quantify this theoretically, the potential entropic benefit of solvent exclusion at the TCR–pHLA interface could also be relevant to the increased binding affinity reported.[13]

Higher specificity of the clinical TCR is encoded in its CDR loop sequences and local structure

During our discovery/engineering programs, we routinely generate multiple TCR candidates. It is critical to select optimal TCR(s) not only for improved affinity and functional potency, but also for the highest specificity. As described previously,[13] Adaptimmune's two leading therapeutic candidates targeting MAGE-A10 were ultimately distinguished by X-scan peptide selectivity profiling. This revealed that the second leading engineered TCR from a different parent, termed c756, was potentially the more

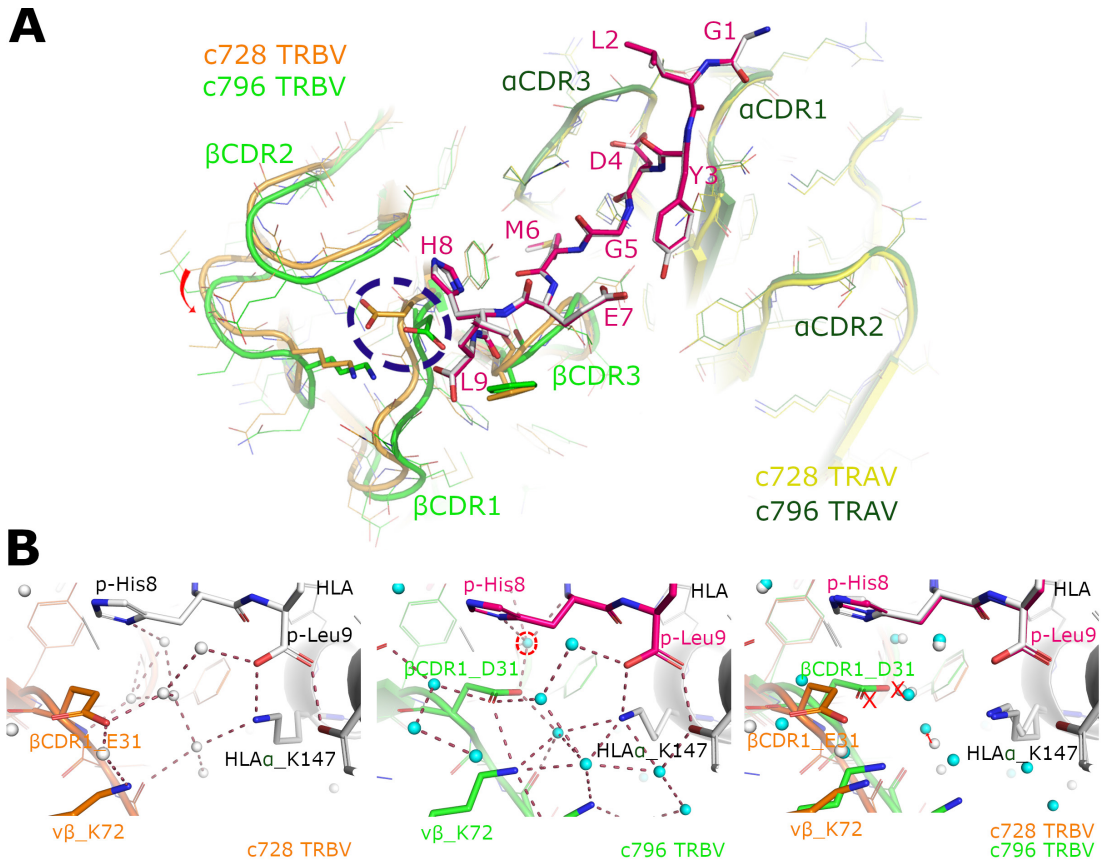

Figure 3 Comparison of peptide–human leucocyte antigen (pHLA) docking between parental (c728) and engineered (c796) T-cell receptors (TCRs). Complexes were superimposed based on an HLA α-chain peptide-binding domain superposition (residues 1–180). (A) View depicting how the peptide sits on the TCR binding interface. It is striking how aligned the peptides are, as well as the TCR alpha chain variable domains; the shorter E31D side-chain in the engineered c796 TCR mutation flips toward the pHLA and brings with it all β complementarity-determining region (CDR) loops in a rigid-body movement (the dashed blue oval shows the mutation site). The HLA is removed for clarity. CDR loop and peptide labels adopt the color scheme of the c796 TCR complex (see below). (B) Detail around the C-terminus of the peptide for pHLA complexed to c728 (left panel) or c796 (middle panel); HLA is above and TCR below. The two TCR–pHLA complexes are shown superimposed (right panel). An invariant water molecule bridging p-His8 and HLA is shown (middle panel; red dashed circle), which the c796 TCR E31D mutant can twist toward and latch on to, pulling with it the TCR beta chain variable domain (TRBV) Lys72 (Vβ_K72). This Lys72 indirectly links to HLA through another bridging water, which was too far in the parental TCR complex. Color scheme: HLA α-chain (gray); c728 complex: TRBV (orange), solvent/water molecules (white spheres), peptide (white sticks); c796 complex: TRBV (green), water molecules (cyan spheres), peptide (pink sticks); H-bonding opportunities shown for the individual complexes (raspberry-colored dashes, left and middle panels). Red crosses (X; right panel) emphasize the loss of interfacial solvent molecules in the engineered c796 TCR–pHLA complex, and the small red arrow shows a displacement of 1 water molecule in the c796 complex relative to its position in the c728 complex. Images generated with PyMOL (Schrödinger, New York, New York, USA).

cross-reactive despite being slightly less potent, driving our choice for progressing with c796 TCR.

The two rival TCRs (c796 and c756) share a common TRAV12-2 α-chain with only two CDR1 or 2 loop differences, namely additional engineered Q32S and S53A substitutions in c756, but they included an identical αCDR3 region. However, the βCDR loops, although TRBV6-5 in origin, had non-identical βCDR3 loop sequences, and c756 lacked the engineered βCDR1 E31D mutation described above for c796. We postulated, therefore, that any sequence differences at the binding interface—the different β-chain in particular—might have contributed to the lower selectivity of c756.

To better visualize this, we crystallized c756 TCR in complex with pHLA/MAGE-A10-9 and compared the molecular details at the TCR–peptide binding interface with those observed in the c796–pHLA/MAGE-A10-9 complex. Again, single crystals grew from the c756–pHLA/MAGE-A10-9 complex, one of which diffracted to beyond 1.54 Å. This resolution is uncommonly high for a TCR–pHLA complex, offering a more precise view of the molecular interactions at the binding interface. At the time of writing, it was the second-highest resolution TCR–pHLA complex structure to be deposited in the PDB.[31]

Superimposition of this complex on the c796 TCR–pHLA/MAGE-A10-9 complex allowed a close comparison of their binding modes. First, the way in which

αCDR3 engages with the central peptide portion is very similar to c728 and c796, and not unexpected given their 100% shared sequence identities. However, the different βCDR3 in c756 has a key effect: it twists away from the TRAV αCDR3, opening a central cavity at and around the base of where peptide p-Met6 plugs in (ie, sculpting a wider and deeper cavity; figures 4B and 5). Our previously reported X-scan demonstrated that the central peptide residues Asp[4]-Gly[5]-Met[6] could be swapped one at a time to a greater number of other amino acids and still elicit functional responses with c756 TCR (ie, c756 tolerated more variants of the cognate peptide; figure 4A).[13]

By modeling substitutions in the structure, it was apparent that the larger cavity allows the branched amino acid Leu to be accommodated without impacting the βCDR3 position (not shown). In the c796 TCR complex the βCDR3 backbone and side-chains close up this cavity to some extent around the wild-type MAGE-A10 peptide, whereas additional water molecules in the c756 complex are observed in the central cavity. The p-Gly5 position benefits from a new cavity just underneath in which smaller side-chains might be accommodated consistent with previous X-scan data.[13] We note that the extra c756 TCR internal spaces may simply allow expansion of the peptide volume, yet prevented from happening by the space-filling rigidity of c796 TCR (figure 5). The binding interface is also affected by the Q32S substitution unique to c756 αCDR1, which again manifests a similar effect: the reduction in serine side-chain volume leaves a less occluded surface close to peptide residue p-Asp4. The αCDR2 S53A mutation on c756, however, is distant from the peptide–TCR interaction site and appears to be of no consequence to specificity differences (figures 4B and 5).

The c756 TCR TRBV has an altered surface charge, from negative to neutral in the contact region with the MAGE-A10 C-terminus, near to p-His8 (figure 4B). The reported X-scan showed c756 TCR was permissive to an increased number of mainly smaller non-charged residues at that peptide position (figure 4A),[13] complementary to this surface. An electrostatic potential surface for the whole pHLA reveals close charge complementarity between key peptide residues interacting with c796 TCR (figure 4D). Where complementarity is less well matched, it seems the solvent structure may compensate to further stabilize the interaction, as discussed above (figures 3B and 4C).

DISCUSSION

The clinical efficacy in solid tumor settings of adoptive T-cell therapies (eg, targeting NY-ESO-1, MAGE-A4, and others) has highlighted the potential benefits to patients of TCR T-cell therapies. However, the deaths of a small number of patients in certain TCR-based immunotherapy trials have highlighted the danger of unrecognized cross-reactivity. Understanding better the specificity of TCRs for their cognate peptide–HLA targets and what may govern potential off-target peptides is therefore critical for their safe therapeutic application. It is clear we should continually improve and refine our safety testing methods as we build our understanding of TCR cross-reactivity/specificity, which is nourished by continual interrogation of the ever-expanding TCR–pHLA structure database.

The literature describes various approaches to explore TCR cross-reactivity and specificity, from experimental library screening methods to computational approaches and predictions (reviewed by Lee *et al*[17]). The fundamental forces governing cross-reactivity/specificity are strongly related to the nature of the interacting surface of the TCR, and to that of the peptide presented by the HLA (major histocompatibility complex) molecule. Although screening methods can profile the potential interactomes (or cross-reactomes) of a given TCR or TCR pair, the fine details of why one TCR has higher specificity than another can only be properly understood by a careful comparative analysis of their individual molecular structures in the context of supporting experimental data. Thus, our study presented the crystal structures of MAGE-A10 TCRs interpreted with respect to previously published biochemical and cell biological data,[13] offering unforeseen explanations for their functional properties.

The MAGE-A10 peptide plugs two protruding residues (p-Asp4, p-Met6) into the TCR 'socket'. One key finding was that sequence differences in the less selective c756 TCR created additional cavities between the TCR and the peptide, compared with the c796 TCR—the basis for Adaptimmune's ADP-A2M10 clinical SPEAR T-cell product. As a result, in specific neighboring positions, substitution of the peptide's amino acids should be more likely with sufficient space to allow a broader set of side-chains. These changes may be accommodated by the TCR without steric repulsion in some cases, or by the central cavity allowing minimal local TCR rearrangements to accommodate the different peptide geometries, while maintaining the overall docking mode.

Altered surface electrostatics (neutralization of a negative charge) in a p-His8-proximal TRBV residue allowed twice the number of side-chains to be reactive toward c756 TCR, essentially those with non-charged, small-length/medium-length side-chains (figure 4A).[13] Therefore, the ability of the MAGE-A10-targeting TCRs to cross-react with non-cognate peptides is most simply explained by the level of complementarity at the TCR–pHLA interface. c796 TCR, with its higher complementarity, offers less room for maneuvering and chemical change in the context of different HLA-bound peptide sequences compared with c756. By extension, structural insights support the notion that amino acid substitutions with space-filling side-chains at CDR positions that do not apparently contribute to functional potency improvements may be more generally useful if they reduce the degrees of freedom around the peptide. In this manner, the repertoire of antigenic peptides with similar sequences tolerated would be more heavily restricted, reducing the likelihood of cross-reactivity, which might depend on the TCR and pHLA in question.

A

	Tolerated amino-acid substitutions at MAGE-A10 GLYDGMEHL peptide position:								
TCR:	1	2	3	4	5	6	7	8	9
c756	GDEHKRNQSTCPAYWFMLV	LNQSTCGAMVI	Y	DCMN	GSTAPHIL	MPGL	EQ	HRQCMLVYNSTPGAFI	LTCFMVI
c796	GDEHKRNQSTCPAYWFMLV	LNQSTCGAMVIF	YF	DC	GST	MP	EQ	HRQCMLVY	LTCFMVIAQ

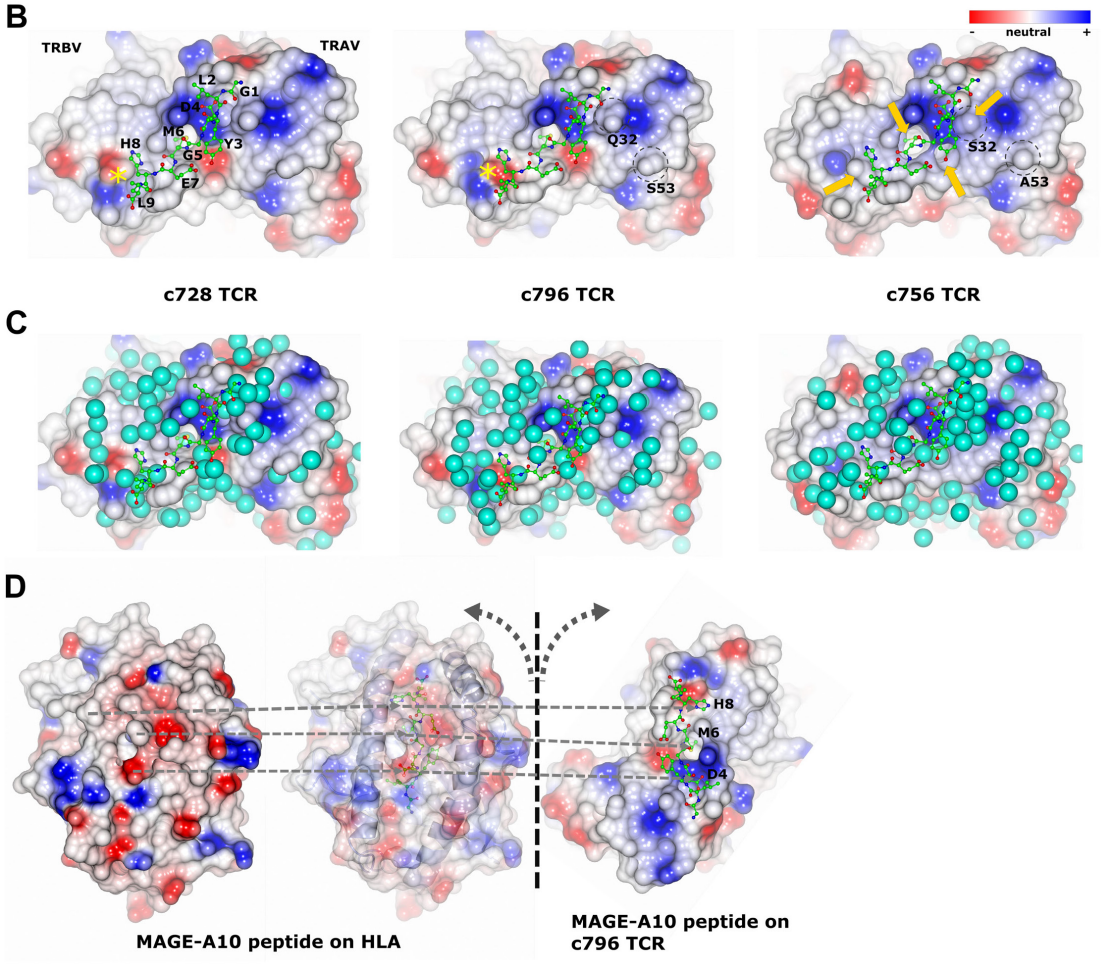

Figure 4 Sequence differences between MAGE-A10 T-cell receptors (TCRs) create different binding surface geometries and electrostatics that can influence potential cross-reactivity. (A) Summarized X-scan motifs for c756 and c796 TCRs (reassembled from Border *et al*[13]). Color code: white background—same residue restriction at a given position; red intensity is proportional to the increased number of amino acids tolerated by one TCR relative to the other. (B) Comparison of three MAGE-A10 TCR–peptide (GVYDGMEHL) interactions; the underlined, bold peptide positions are TCR-facing. Electrostatic surface potential (ESP) representations of TCR bound to MAGE-A10 peptide (green ball-and-stick view) show the central cavity in TCR where p-Met6 docks (ESP coloring: red, negative charge; blue, positive; white, netural). Note, HLA would sit above but is removed from view. The yellow asterisk (left and middle panels) denotes the engineered position of the engineered TRBV E31D mutation. Additional cavities and flanking spaces are available around the peptide's central residues, and electrostatic changes proximal to the penultimate His in c756 TCR (right panel, gold arrows), consistent with its ability to accommodate a wider variety of peptide side-chains. In the middle panel, the two residue positions that differ between the TRAV domains in c796 and c756 TCRs are indicated for c796 TCR (black dashed circles); Q32S and S53A are the substitutions in c756 TCR (right panel), and S32 provides more space by the target peptide. Differences associated with the sequence of c756 TCR TRBV, including neutralization of the TRBV negative charge in c796 (bottom left of image) near to p-His8, permit all the small non-charged or hydrophobic residues to sit at that site in the context of a c756 TCR interaction. (C) ESP views for the TCRs in the same order as in part (B), shown with TCR/MAGE-A10 peptide-proximal solvent structure. The water molecules (cyan spheres) are observed crystallized in that position; note, more distant water molecules above the plane of the peptide are removed from view. There are many water positions in common. Changes occur near to the E/D31 position in c728 and c796 TCRs, and a marked increase in water molecules is seen at the Q32S site in the c756 TCR complex, where the increased space is solvent-filled (right panel). (D) ESP surface of MAGE-A10 peptide–HLA as 100% and 50% opaque views (left and middle panels, respectively) to allow visualization of the enclosed peptide. The pHLA is one half of an 'open book' representation of the full TCR–pHLA complex, with c796 TCR (on the far right) peeled off the pHLA. Note, the MAGE-A10 peptide is shown bound to both HLA and TCR to orient the mapping of key TCR-interacting residues in the -peptide: p-Asp4, p-Met6, and p-His8 (gray dashed lines). ESP surface representations in (B) to (D) were generated using default settings with *CCP4mg*.[50]

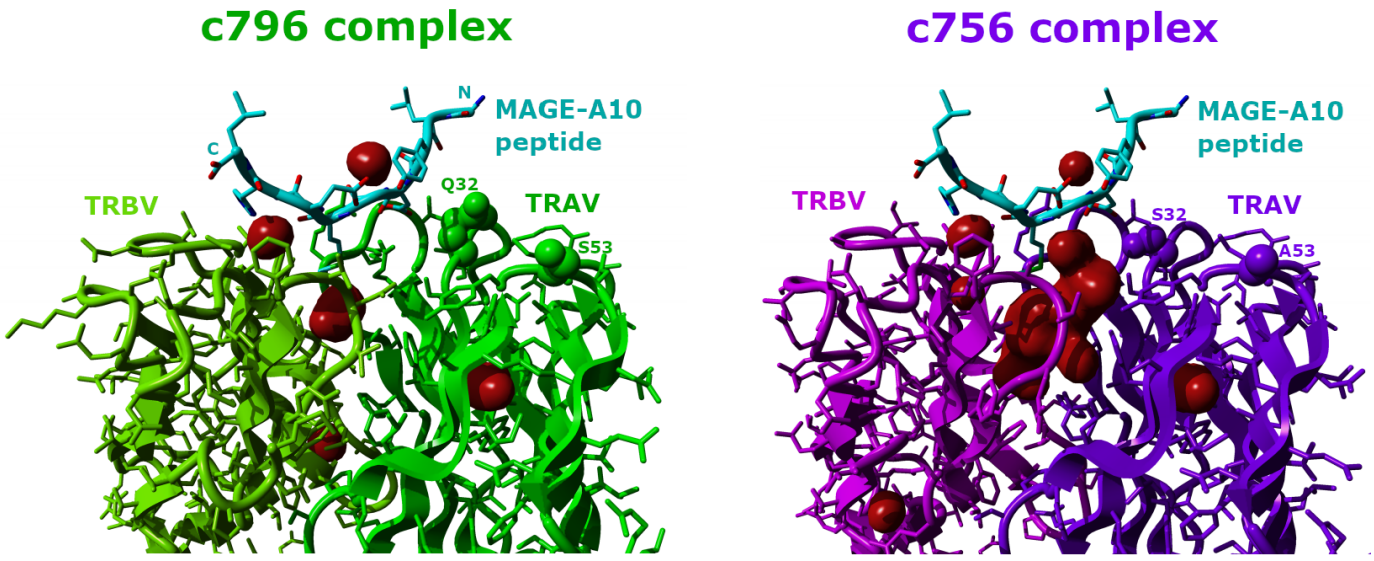

Figure 5 Comparison of internal cavities within engineered T-cell receptors (TCRs) and around melanoma-associated antigen (MAGE)-A10 peptide. Cavities are represented as burgundy blobs and were calculated and represented using YASARA Structure (YASARA Biosciences, Vienna, Austria). The c796 TCR (left panel, green shades) has a more space-filling central region in the TCR variable domain interface, largely caused by β complementarity-determining region (CDR)3_D98 (not highlighted) which extends between the TCR variable domains bonding to human leucocyte antigen (HLA) alpha chain Q156 and adjacent to αCDR3_R93 (note, the HLA molecule is not depicted in the view, but would be positioned above). Thus, the central cavity of the complexed c796 TCR is relatively small compared with that of c756 TCR (right panel, purple shades)—its βCDR3 loop taking on a different trajectory, with a Thr residue at the 98 position, incapable of bonding to HLA or TCR alpha chain variable domain (TRAV) in the same manner. The additional total cavity volume in c756 TCR suggests that differences within the HLA-bound peptide should be more easily accommodated either directly, or by the greater freedom of movement of the TCR CDR3 loops presumably allowed, consistent with the reported X-scan data (figure 4A). The chain-colored spheres depict the two TRAV12-2 residues that are non-identical between the two TCRs: Q32S and S53A in c756 relative to c796 TCR. The former substitution reduces some space-filling volume close to the MAGE-A10 peptide, which becomes filled with solvent in the crystal structure (figure 4C, right panel). The more distant S53A substitution appears to have no direct influence on TCR–peptide interactions.

This phenomenon might be related to the observation that the number of residues involved in a TCR–pHLA interaction correlates with cross-reactivity. Evidence suggests that the lower the number of direct binding sites, the more cross-reactive the TCR is likely to be.[32] Given that TCRs are by their nature cross-reactive,[33] it is possible that higher affinity and indeed additional binding specificity to other peptides may arise with a TCR that does not maximize the interfacial space-filling around its cognate antigen. However, the number of hotspot residues contributing binding energy may need balancing, so as not to reach too high an affinity for optimal functionality in the context of a cell–cell interaction.

Since cross-reactivity to a single off-target off-tumour peptide–HLA is sufficient to render a potential T-cell therapy unsafe,[5 6] extensive preclinical cell-panel testing and carefully controlled dose-escalation studies are vital. One useful approach has been the X-scan method, which interrogates single amino acid changes along the peptide. Though informative, this method only covers a small fraction of the potential cross-reactome. For example, the X-scan cannot identify orthogonal binding modes, and hence a broader approach is important, including extensive screening of TCR T-cells on cell lines and primary cells, with other methods available.[34–36] In theory, any TCR could adopt orthogonal binding modes, but it seems logical that the likelihood would be reduced for more rigid TCRs, with specificity tailored to a distinctive target surface. This should be especially true when a target peptide contains more pronounced, irregular features, as opposed to flatter, less varied peptide structures[37] (eg, composed of small, non-polar residues). Optimizing the TCR interaction and surface complementarity does not preclude off-target binding, yet this should reduce the probability that there is another suitable surface to bind to differentially. Prioritizing TCR–pHLA systems with such properties and building in specificity to the most variable portion (ie, the peptide) would seem productive.

The structure-guided design approach may permit refined specificity/cross-reactivity control,[38] especially if off-target cross-reactivities are known. This has been demonstrated for DMF5 TCR engineering[39 40] and attempted for re-engineering a MAGE-A3 TCR to reduce off-target Titin peptide cross-reactivity[6]; other examples are known (eg, those described by Spear *et al*[41]).

With respect to intrinsic structural protein properties the first structural view of HLA-A*02:01/MAGE-A10, reported herein, revealed how p-Tyr3 H-bonds to p-Glu7 within the peptide chain embedded in the HLA peptide-binding groove. The resultant conformation created a

non-covalent side-chain 'self-staple'. This is reminiscent of the related MAGE-A4 peptide local structure (PDB code: 1I4F[26]), which displays a p-Tyr3 to p-Arg6 intra-chain electrostatic interaction, also tucked into the groove, but the tyrosyl ring H-bond reaches to the backbone N or O of p-Arg6. The MAGE-A4 peptide in the pHLA alone (PDB code: 1I4F[26]) or when bound to TCR (PDB code: 6TRO[42]) maintains its docked position on TCR ligation except for expected local side-chain rearrangements on the TCR-facing edge.

These peptide structures with apparent self-stabilization and larger direct contact area within the HLA-binding groove might be expected to impart greater stability to the pHLA complex, and this has been confirmed by in vitro experimental work (our unpublished data; EC Border and S Bruton, personal communication). There are limited other parallels with the MAGE-A4 pHLA structure due to the MAGE-A4 10-mer peptide adopting a central bulge to accommodate the additional amino acid. This influenced the off-center docking location over the peptide's N-terminus of the reported GVY01 TCR,[42] unlike the central position of the MAGE-A10 TCR set presented here.

Another finding was that the parental TCR (c728) maintained a near-identical TRAV conformation before and after pHLA engagement, with all but local side-chain rearrangements. There was a little more movement in the TRBV loops, but it was a minor rigid-body rotation that appeared to enable optimal pHLA docking. The maintenance of CDR loop positions between free and pHLA-ligated structures suggests in-built loop rigidity. In other words, a preferred or dominant conformation would exist in the TCR (or TCR population)—that is, predetermined even before pHLA engagement. It has become apparent from the growing TCR–pHLA structure database that CDR loop flexibility, which can contribute to cross-reactivity,[43] is sequence-specific rather than a universal TCR feature (eg, as described by Holland *et al*[44]). It stands to reason that lower inherent conformational flexibility should restrict promiscuity of binding and may be a useful metric when triaging discovery TCRs, if structural information is available.

Outside the scope of this analysis, but an interesting follow-up, would be to analyze the energetic landscape of the parental and engineered TCRs by molecular dynamics simulations as described,[45 46] and to compare TCR loop conformations using solution methods (eg, nuclear magnetic resonance spectroscopy), as reported.[47] It would also be intriguing to understand whether deep-learning approaches, such as implemented in *AlphaFold 2* (DeepMind)[48] with great success at structure prediction in the CASP14 contest,[31] could reproduce more authentic CDR loop sequence topologies by learning rules governing which sequence combinations encode intrinsically more rigid structures. By understanding more fully the TCR rigidity/flexibility issue for structure-based design, we might better predict positional coordinates and functional characteristics.

CONCLUSION

These new protein structures have illuminated our understanding of functional engineering and specificity data as well as differences in TCR cross-reactivity profiles. Adaptimmune's MAGE-A10-targeting TCR product, originating from in vitro phage display libraries and affinity-enhanced by engineering, has displayed a manageable safety profile in clinical studies. This is the ultimate test of specificity, which validates the development approach taken of TCR affinity enhancement. We associate the beneficial physicochemical features within the engineered c796 TCR–pHLA complex structure with fundamental contributions to its safer in vivo profile.

Correction notice This article has been corrected since it was first published online. BCDR2 residue E53 has been corrected to bCDR1 E31 throughout the article.

Acknowledgements The authors acknowledge the support of staff at Medical Research Council Research Complex at Harwell (Harwell, UK) for crystallization experiments and staff at Diamond Light Source Industrial Liaison Unit (Oxfordshire, UK) for their X-ray data collection service. Thanks to Karen Miller, Chris Herring, and Jaimin Shah for helpful comments on the manuscript. Writing and editorial support for this manuscript was funded by Adaptimmune and was provided by Gabrielle Knafler and Nathaniel Hoover of Excel Scientific Solutions (Fairfield, Connecticut, USA).

Contributors PCS designed and performed the study, analyzed and interpreted the data, wrote the manuscript, and is responsible for the overall content as the guarantor. ECB provided materials and contributed to data interpretation and manuscript revisions. JFV and NJP helped design the study and contributed to data interpretation and manuscript revisions.

Funding Adaptimmune wholly funded this work.

Competing interests All authors are or have been employees of Adaptimmune and may hold shares or share options in the company. Adaptimmune has a patent on the T-cell receptors mentioned in this study with ECB a named coinventor.

Patient consent for publication Not applicable.

Provenance and peer review Not commissioned; externally peer reviewed.

Data availability statement Data are available in a public, open access repository. Refined crystal structure models and experimental data have been deposited in the PDB[49] with the following accession codes: 7PDX (c728 TCR), 7PDW (c728 TCR–HLA-A*02:01/MAGE-A10-9 complex), 7PBC (c796 TCR–HLA-A*02:01/MAGE-A10-9 complex), and 7QPJ (c756 TCR–HLA-A*02:01/MAGE-A10-9 complex).

REFERENCES

1 Simpson AJG, Caballero OL, Jungbluth A, *et al*. Cancer/Testis antigens, gametogenesis and cancer. *Nat Rev Cancer* 2005;5:615–25.
2 Zhang J, Wang L. The emerging world of TCR-T cell trials against cancer: a systematic review. *Technol Cancer Res Treat* 2019;18:153303381983106.
3 Clinical studies including MAGE-A10 as a target. Available: https://clinicaltrials.gov/ct2/results?cond=&term=MAGE-A10 [Accessed 12 April 2022].
4 Weon JL, Potts PR. The MAGE protein family and cancer. *Curr Opin Cell Biol* 2015;37:1–8.
5 Morgan RA, Chinnasamy N, Abate-Daga D, *et al*. Cancer regression and neurological toxicity following anti-MAGE-A3 TCR gene therapy. *J Immunother* 2013;36:133–51.
6 Raman MCC, Rizkallah PJ, Simmons R, *et al*. Direct molecular mimicry enables off-target cardiovascular toxicity by an enhanced

affinity TCR designed for cancer immunotherapy. *Sci Rep* 2016;6:18851.
7 Wolf B, Zimmermann S, Arber C, *et al*. Safety and tolerability of adoptive cell therapy in cancer. *Drug Saf* 2019;42:315–34.
8 Løset GA, Berntzen G, Frigstad T, *et al*. Phage display engineered T cell receptors as tools for the study of tumor peptide-MHC interactions. *Front Oncol* 2014;4:378.
9 Smith SN, Harris DT, Kranz DM. T cell receptor engineering and analysis using the yeast display platform. *Methods Mol Biol* 2015;1319:95–141.
10 Manfredi F, Cianciotti BC, Potenza A, *et al*. TCR redirected T cells for cancer treatment: achievements, hurdles, and goals. *Front Immunol* 2020;11:1689.
11 Hong DS, Van Tine BA, Olszanski AJ, *et al*. Phase I dose escalation and expansion trial to assess the safety and efficacy of ADP-A2M4 SPEAR T cells in advanced solid tumors. *J Clin Oncol* 2020;38:102.
12 Blumenschein G, Devarakonda S, Johnson M, *et al*. Phase I clinical trial evaluating the safety of ADP-A2M10 spear T-cells in patients with MAGE-A10+ advanced non-small cell lung cancer (Abstract 278). *J Immunother Cancer* 2020;8:A169–70.
13 Border EC, Sanderson JP, Weissensteiner T, *et al*. Affinity-enhanced T-cell receptors for adoptive T-cell therapy targeting MAGE-A10: strategy for selection of an optimal candidate. *Oncoimmunology* 2019;8:e1532759.
14 Sanderson JP, Crowley DJ, Wiedermann GE, *et al*. Preclinical evaluation of an affinity-enhanced MAGE-A4-specific T-cell receptor for adoptive T-cell therapy. *Oncoimmunology* 2020;9:1682381.
15 Bijen HM, van der Steen DM, Hagedoorn RS, *et al*. Preclinical strategies to identify off-target toxicity of high-affinity TCRs. *Mol Ther* 2018;26:1206–14.
16 Cai L, Caraballo Galva LD, Peng Y, *et al*. Preclinical Studies of the Off-Target Reactivity of AFP_{158}-Specific TCR Engineered T Cells. *Front Immunol* 2020;11:607.
17 Lee CH, Salio M, Napolitani G, *et al*. Predicting cross-reactivity and antigen specificity of T cell receptors. *Front Immunol* 2020;11:565096.
18 Hong DS, Butler MO, Pachynski RK, *et al*. Phase 1 clinical trial evaluating the safety and anti-tumor activity of ADP-A2M10 spear T-cells in patients with MAGE-A10+ head and neck, melanoma, or urothelial tumors. *Front Oncol* 2022;12:818679.
19 Blumenschein GR, Devarakonda S, Johnson M, *et al*. Phase I clinical trial evaluating the safety and efficacy of ADP-A2M10 SPEAR T cells in patients with MAGE-$A10^{+}$ advanced non-small cell lung cancer. *J Immunother Cancer* 2022;10:e003581.
20 Winn MD, Ballard CC, Cowtan KD, *et al*. Overview of the CCP4 suite and current developments. *Acta Crystallogr D Biol Crystallogr* 2011;67:235–42.
21 Battye TGG, Kontogiannis L, Johnson O, *et al*. iMOSFLM: a new graphical interface for diffraction-image processing with MOSFLM. *Acta Crystallogr D Biol Crystallogr* 2011;67:271–81.
22 Winter G, Waterman DG, Parkhurst JM, *et al*. DIALS: implementation and evaluation of a new integration package. *Acta Crystallogr D Struct Biol* 2018;74:85–97.
23 Winter G. *xia2*: an expert system for macromolecular crystallography data reduction. *J Appl Crystallogr* 2010;43:186–90.
24 Evans PR, Murshudov GN. How good are my data and what is the resolution? *Acta Crystallogr D Biol Crystallogr* 2013;69:1204–14.
25 McCoy AJ, Grosse-Kunstleve RW, Adams PD, *et al*. *Phaser* crystallographic software. *J Appl Crystallogr* 2007;40:658–74.
26 Borbulevych OY, Santhanagopolan SM, Hossain M, *et al*. TCRs used in cancer gene therapy cross-react with MART-1/Melan-A tumor antigens via distinct mechanisms. *J Immunol* 2011;187:2453–63.
27 Hillig RC, Coulie PG, Stroobant V, *et al*. High-Resolution structure of HLA-A*0201 in complex with a tumour-specific antigenic peptide encoded by the MAGE-A4 gene. *J Mol Biol* 2001;310:1167–76.
28 Murshudov GN, Skubák P, Lebedev AA, *et al*. REFMAC5 for the refinement of macromolecular crystal structures. *Acta Crystallogr D Biol Crystallogr* 2011;67:355–67.
29 Emsley P, Lohkamp B, Scott WG, *et al*. Features and development of *Coot*. *Acta Crystallogr D Biol Crystallogr* 2010;66:486–501.
30 Chen VB, Arendall WB 3rd, Headd JJ, *et al*. MolProbity: all-atom structure validation for macromolecular crystallography. *Acta Crystallogr D Biol Crystallogr* 2010;66:12–21.
31 University of California, Davis. CASP14. Available: https://www.predictioncenter.org/casp14 [Accessed 12 April 2022].
32 Cole DK, van den Berg HA, Lloyd A, *et al*. Structural mechanism underpinning cross-reactivity of a CD8+ T-cell clone that recognizes a peptide derived from human telomerase reverse transcriptase. *J Biol Chem* 2017;292:802–13.
33 Sewell AK. Why must T cells be cross-reactive? *Nat Rev Immunol* 2012;12:669–77.
34 Gee MH, Han A, Lofgren SM, *et al*. Antigen identification for orphan T cell receptors expressed on tumor-infiltrating lymphocytes. *Cell* 2018;172:549–63.
35 Riley TP, Hellman LM, Gee MH, *et al*. T cell receptor cross-reactivity expanded by dramatic peptide-MHC adaptability. *Nat Chem Biol* 2018;14:934–42.
36 Coles CH, Mulvaney RM, Malla S, *et al*. TCRs with distinct specificity profiles use different binding modes to engage an identical peptide-HLA complex. *J Immunol* 2020;204:1943–53.
37 Antunes DA, Rigo MM, Freitas MV, *et al*. Interpreting T-cell cross-reactivity through structure: implications for TCR-based cancer immunotherapy. *Front Immunol* 2017;8:1210.
38 Riley TP, Ayres CM, Hellman LM, *et al*. A generalized framework for computational design and mutational scanning of T-cell receptor binding interfaces. *Protein Eng Des Sel* 2016;29:595–606.
39 Hellman LM, Foley KC, Singh NK, *et al*. Improving T cell receptor on-target specificity via structure-guided design. *Mol Ther* 2019;27:300–13.
40 Malecek K, Grigoryan A, Zhong S, *et al*. Specific increase in potency via structure-based design of a TCR. *J Immunol* 2014;193:2587–99.
41 Spear TT, Evavold BD, Baker BM, *et al*. Understanding TCR affinity, antigen specificity, and cross-reactivity to improve TCR gene-modified T cells for cancer immunotherapy. *Cancer Immunol Immunother* 2019;68:1881–9.
42 Coles CH, McMurran C, Lloyd A, *et al*. T cell receptor interactions with human leukocyte antigen govern indirect peptide selectivity for the cancer testis antigen MAGE-A4. *J Biol Chem* 2020;295:11486–94.
43 Piepenbrink KH, Blevins SJ, Scott DR. The basis for limited specificity and MHC restriction in a T cell receptor interface. *Nat Commun* 1948;2013:4.
44 Holland CJ, MacLachlan BJ, Bianchi V, *et al*. *In Silico* and Structural Analyses Demonstrate That Intrinsic Protein Motions Guide T Cell Receptor Complementarity Determining Region Loop Flexibility. *Front Immunol* 2018;9:674.
45 Crean RM, MacLachlan BJ, Madura F, *et al*. Molecular rules underpinning enhanced affinity binding of human T cell receptors engineered for immunotherapy. *Mol Ther Oncolytics* 2020;18:443–56.
46 Kass I, Buckle AM, Borg NA. Understanding the structural dynamics of TCR-pMHC complex interactions. *Trends Immunol* 2014;35:604–12.
47 Fernández-Quintero ML, Pomarici ND, Loeffler JR, *et al*. T-Cell receptor CDR3 loop conformations in solution shift the relative Vα-Vβ domain distributions. *Front Immunol* 2020;11:1440.
48 Jumper J, Evans R, Pritzel A, *et al*. Highly accurate protein structure prediction with AlphaFold. *Nature* 2021;596:583–9.
49 Berman HM, Westbrook J, Feng Z, *et al*. The protein data bank. *Nucleic Acids Res* 2000;28:235–42.
50 McNicholas S, Potterton E, Wilson KS, *et al*. Presenting your structures: the CCP4mg molecular-graphics software. *Acta Crystallogr D Biol Crystallogr* 2011;67:386–94.